Article:
Hua, Y, Barker, R orcid.org/0000-0002-5106-6929 and Neville, A orcid.org/0000-0002-6479-1871 (2015) The influence of SO_2 on the tolerable water content to avoid pipeline corrosion during the transportation of supercritical CO_2. International Journal of Greenhouse Gas Control, 37. pp. 412-423. ISSN 1750-5836

https://doi.org/10.1016/j.ijggc.2015.03.031

The influence of SO_2 on the tolerable water content to avoid pipeline corrosion during the transportation of supercritical CO_2

Yong Hua, Richard Barker and Anne Neville
Institute of Functional Surfaces
School of Mechanical Engineering
University of Leeds
Leeds
LS2 9JT
United Kingdom

Corresponding author: Yong Hua, Tel: +44 (0) 7923359918, fax: +44 (0) 1132424611.
Email: mnyh@leeds.ac.uk

Abstract

A systematic study is undertaken to establish the influence of sulphur dioxide (SO_2) concentration on the critical water content required to avoid substantial levels of internal corrosion during the transport of supercritical CO_2 for carbon capture and storage (CCS) applications. Corrosion experiments were performed on X65 carbon steel in autoclaves containing supercritical CO_2 at 80 bar and 35°C in the presence of 0, 50 and 100 ppm (mole) SO_2. General and localised corrosion rates were determined over a period of 48 hours through the implementation of gravimetric analysis and surface profilometry, respectively. Analysis of corrosions products formed on the steel surface was performed using x-ray diffraction, Raman spectroscopy and scanning electron microscopy. The results indicate that the presence of SO_2 reduces the critical water content required to maintain a general corrosion rate below 0.1 mm/year. Furthermore, the water content required to avoid excessive localised corrosion is far less than that to prevent significant general corrosion. Localised corrosion rates close to 1 mm/year were observed in the absence of SO_2 when the CO_2 system was water-saturated, but below water contents of ~1800 ppm (mole) and ~500 ppm, general and localised corrosion rates (respectfully) were found to be below 0.1 mm/year even in the presence of 100 ppm SO_2. The research presented highlights that reducing water content is a more favourable option compared to reducing SO_2 content to minimise internal pipeline corrosion during transportation. Consideration is also afforded to the consumption of impurities in the closed system experiments.

Keywords: corrosion, pitting, CO_2 transport, iron carbonate, iron sulphite

1. Introduction

The widespread implementation of Carbon Capture and Storage (CCS) technology would enable the continued use of fossil fuels through the abatement of CO_2, preventing emissions

into the atmosphere. Currently, CCS is the only technology which has the potential to make a significant and immediate impact on reducing the CO_2 level in the environment.

CCS involves capturing CO_2 from large point sources (e.g. power generation, refineries and other industrial applications), compressing the gas into a liquid or supercritical state and transporting it to geological reservoirs or depleted oil and gas reservoirs for sequestration or enhanced oil recovery (EOR) purposes.

It is predicted that, for the abatement of climate change, approximately 10 Gt/year of CO_2 will need to be transported and sequestered in 2050[1]. Dugstad et al.[1] estimated that this would require the construction of 3000 twelve-inch (or 1000 twenty-inch) pipelines under the assumption of a flow velocity of 1.5 m/s. They suggested that the only logical choice to achieve such enormous levels of abatement would be to have an extensive pipeline network constructed from carbon steel.

The transportation of CO_2 has been practiced for over 30 years and currently, over 6000 km of pipeline exist for EOR purposes. The majority of these pipelines are located in the USA and Canada, with some projects also being undertaken in Norway. Most of these pipelines transport CO_2 from natural sources, with a few pipelines carrying anthropogenic CO_2 as shown in Table 1.

Although the composition of CO_2 streams is not readily available in open literature, Table 1 provides a summary of information compiled from various sources[2, 3, 4, 5, 6, 7, 8]. CO_2 from natural sources is typically high purity and will require minimal gas treatment prior to injection. Only impurities such as CO_2, N_2, CH_4, H_2O and H_2S are to be expected[9]. Considering anthropogenic sources, there can be a distinct difference in fluid composition, as the stream can become further contaminated as a result of the presence of flue gas impurities (SO_x, NO_x and O_2 in particular). Regrettably, this is not reflected in the list of anthropogenic sources in Table 1, and it is unclear from open literature whether this is because these components are not present in the CO_2 stream or that the process fluid was not analysed for these particular compounds.

Nonetheless, there will be significant differences between the transport of natural CO_2 and CO_2 from anthropogenic sources. Flue gas impurities are to be expected and will vary depending upon the type of capture process, the source and the level of gas treatment applied. Table 2 is adapted from the work of Lee et al.[10] who considered five different scenarios of post processing methodologies for a coal-fired power station with different levels of proposed contaminants. The table provides an example of the significant variations in impurity levels depending upon the amount of post processing involved in terms of coal combustion.

As shown in Table 1, it can be observed that the water contents within each CO_2 stream vary from ~20 ppm (mole) to ~630 ppm (mole), with the exception of Sleipner which could be regarded as an anomaly in that it carries water-saturated supercritical CO_2 using pipelines constructed from corrosion resistant alloys. Unfortunately, little information has been published on the rationale behind these imposed concentration limits.

If the water content within the CO_2 stream exceeds the solubility limit locally, a separate aqueous phase will exist. If such a phase were to form on the pipeline wall, it will invariably become saturated with CO_2, forming carbonic acid (H_2CO_3), lowering the pH of the aqueous phase (to pH ~3.3 at 80 bar) and posing a threat to pipeline integrity, even without the presence of additional flue gases such as SO_x and NO_x.[11]

It is worth noting in Table 1 that the two anthropogenic sources from gasification plants possess some of the lowest water specifications to prevent the break-out of water and the potential onset of corrosion. The introduction of impurities such as SO_x, O_2, and NO_x from flue gases can pose a significant problem for the transportation of anthropogenic CO_2 streams in terms pipeline integrity when a sufficient level of water is present in the system to generate an aqueous phase[1]. When SO_2 and O_2 in particular are all present in the system, they can segregate into the aqueous phase forming sulphurous (H_2SO_3) and/or sulphuric acid (H_2SO_4), further lowering the pH and potentially increasing the corrosivity of the environment.[1]

Consequently, to mitigate against the inherent risk associated with corrosion, pipeline operators set their own limits for water content in CO_2 streams. According to Aspelend et al.,[12] and Dugstad et al.,[1] 500 ppm was considered to be the accepted limit in literature, although little reasoning exists behind this specific value. Kinder Morgan set a concentration limit of approximately 600 ppm[13], the CO_2 stream at Weyburn is dehydrated down to 20 ppm whilst the pipelines at Sleipner transport water-saturated CO_2 but use a corrosion resistant alloy as the pipeline material, as previously mentioned[14]

Surprisingly, there is no general consensus on what the actual allowable water content should be in the transported CO_2 stream[1]. Furthermore, limited information exists in literature relating to the impact of impurities (other than water) on the corrosion processes in supercritical CO_2 systems where CO_2 is the dominant phase. A review of the work by Dugstad et al.,[1, 15] Hua et al.,[16, 17, 18] and Sim et al.,[19] indicates that localised corrosion of carbon steel is significant in dense phase CO_2 with only water as impurity. Hua et al.,[16, 17] indicated that no localised attack was observed at 300 and 1600 ppm of water in supercritical CO_2 condition (35°C and 50°C and 80 bar, respectively).

Some other valuable work was performed by Choi et al.[13, 20] who considered the effect of impurities of 4% O_2 and 1% SO_2 on the degradation of carbon steel in supercritical CO_2 at 80 bar and 50°C. Choi et al.[13, 20] evaluated the corrosion behaviour of X65 steel in both the water-saturated CO_2 phase and with the presence of only 650 ppm water. Their research highlighted that the corrosion rates could reach ~7 mm/year in the most severe conditions tested (water-saturated with the addition of 4% O_2 and 1% SO_2).

Dugstad and co-workers[21] performed long durations experiments (7 and 30 days) to evaluate the susceptibility of X65 steel to corrosion in the presence of O_2 (0-200 ppm) and SO_2 (0-1000 ppm) at 100 bar and 20°C. Their findings indicated that the combined presence of O_2 (100 ppm) and SO_2 (200 ppm) induced small levels of corrosion (~0.01 mm/year) at water contents of 488 ppm, whilst no corrosion was observed at a higher water content of 1220 ppm when O_2 and SO_2 were absent from the system.

Farelas et al.[22] considered the influence of a phase change of CO_2 from a supercritical fluid to liquid on the corrosion of X65. They determined that at 80 bar in static, liquid CO_2 conditions (25°C) corrosion was much more prevalent with the addition of 650 ppm water and 0.05% SO_2 than at supercritical conditions (50°C) with the same levels of impurities.

Finally, Xiang et al.[14, 23, 24] have performed a handful of key studies which have considered the influence of SO_2 content (0.2-2 bar) on the corrosion rate of X70 carbon steel in water-saturated and under-saturated supercritical CO_2[23] as well as the influence of exposure time[14] and water content[24]. A summary of the aforementioned results were compiled by Hua et al.,[25] and are provided in another publication.

Although one particular publication by Xiang et al.[24] involved assessing the corrosion behaviour of X70 carbon steel through varying water content in the presence of 2% SO_2 in supercritical CO_2 at 100 bar and 50°C, no systematic study has been conducted currently in literature to attempted to establish whether the same behaviour observed (in terms of the critical water content required to induce corrosion) extends to lower impurity systems, nor has the corrosion rate been quantified through localised corrosion measurements in such environments.

The research presented in this study has two key goals; firstly, to determine the influence of SO_2 contents typical of the CO_2 stream on the susceptibility of carbon steel to both general and localised corrosion in supercritical environments both under-saturated and saturated with water; and secondly, to determine the role of SO_2 content on the critical water content required to ensure no appreciable levels of corrosion are observed. For the purposes of this work, the threshold for the water content is defined as the point below which the corrosion rate (general or localised) is below 0.1 mm/year.

General and localised corrosion rates reported in this study are evaluated through a combination of the weight loss method and surface profilometry, respectively. Furthermore, a detailed analysis of the corrosion products formed in each environment is not presented here, although a selection of SEM images and XRD patterns are provided to show the morphology and composition of the corrosion products in specific experiments and how these are influenced by the presence of SO_2.

2. Experimental procedure

2.1 Materials and preparation

Test specimens were machined from carbon steel bars (API 5L X65) into discs of diameter 25 mm and thickness of 6 mm. The chemical composition of the X65 steel is provided in Table 3. Surface preparation consisted of wet-grinding the entire sample up to 800 grit using silicon carbide abrasive paper, rinsing with distilled water, followed by acetone, high purity ethanol and drying gently with compressed air. Samples were then stored in a desiccator until needed and weighed immediately before the experiment on an electronic balance with an accuracy of 0.001 mg before suspending inside the autoclave. Two samples were placed within the autoclave for each individual test, generating a total surface area of approximately 27 cm^2 exposed to the dense-phase CO_2.

2.2 Autoclave testing procedure

Figure 1 provides a schematic representation of the experimental system layout. The entire system consists of a 1 litre capacity autoclave, temperature controller, a $CO_2/SO_2/O_2$ mixed cylinder, a series of valves for CO_2 flow control and a waste gas treatment system.

The distilled water used in each experiment was de-aerated by saturating the solution with CO_2 in a separate container for a minimum of 12 hours prior to testing. The specimens were suspended within the autoclave on a non-conducting wire whilst also ensuring they were not in contact with the walls of the cylinder to prevent galvanic effects. The prepared, required amount of CO_2-saturated water was carefully delivered into the autoclave at ambient pressure and temperature and sealed. All lines to the autoclave were purged with CO_2 and evacuated to ensure removal of O_2 within the system. The required $CO_2/SO_2/O_2$ mixture was then transferred into the autoclave and heated and pressurised to the required temperature and pressure. The starting point of the test is taken from the time at which the autoclave reached the required temperature and pressure. At the end of each experiment, the exhaust gas was filtered through an alkali solution to prevent release into the environment.

Based on the model by Spycher et al.[26] the saturated water concentration in supercritical CO_2 at 35°C and 80 bar is 3437 ppm. In order to ensure the water-saturated CO_2 condition, 34000 ppm of water was introduced to the autoclave for the water-saturated tests (i.e. approximately 10 times the saturation limit). For experiments performed in under-saturated conditions, the exact volume of water was determined to achieve each required ppm concentration and this was injected into the bottom of the autoclave using a pipette.

2.3 Determining the test matrix for $SO_2/CO_2/H_2O$ experiments

There are currently no recognised specifications for the CO_2 quality required for transportation[1]. It is envisaged that the main technical constraint imposed will be the maximum allowable impurity content from the perspective of storage or from a corrosion and safety standpoint during transportation.

A number of tentative CO_2 specifications exist in literature, two of which are provided in Table 4 and where used as the basis for selecting the SO_2 concentrations studied within this work. The information within Table 4 was compiled from the European project 'ENCAP – ENhanced CAPture of CO_2' from the DYNAMIS project[7], and a set of data from Alstom adapted from the work of Dugstad et al.,[15]

Although a large variation is observed in tolerated impurity concentrations in Table 2, it is clear that the low limit for SO_2 content is below 100 ppm and is controlled from a health and safety perspective in both specifications. To represent the conditions likely to be encountered in CO_2 streams, SO_2 contents of 0, 50 and 100 ppm were selected in this study. The complete matrix of tests performed within this paper is provided in Table 5, which outline the variations in water content that were also assessed.

At the end of each test conducted within this matrix, the specimens were dried thoroughly and photographed. The samples were subsequently chemically cleaned to remove all traces of corrosion products before weighing. The cleaning process consisted of wiping the surface with a cotton pad soaked in Clarke's solution (20 g antimony trioxide + 50 g stannous chloride + 1000 ml hydrochloric acid) in accordance with ASTM Standard G1-03[27]. This was followed by rinsing the samples with distilled water, followed by drying with compressed air.

The mass loss due to corrosion was determined from the weight difference before exposure and after cleaning. The corrosion rates were calculated by using Equation (1):

$$CR = \frac{87600 \times \Delta m}{\rho \times A \times T} \quad (1)$$

Where CR is the corrosion rate of the sample in mm/y, Δm is the weight loss in grams, ρ is the density of the sample in g/cm^3, A is the exposed area in cm^2 and T is the immersion time in hours.

2.4 Interferometry

The profilometry measurements were performed on samples (scanning a 3 x 3 mm^2 area at a time) using a NP_{FLEX} 3D Surface Metrology System to quantify localised attack. The objective used was 2.5X with a 3.5 mm working distance. All samples that were analysed by profilometry were first cleaned thoroughly with Clarke's solution to remove any traces of corrosion product to enable the pits to be accurately quantified. The pit depth analysis was conducted in accordance with ASTM Standard G46-94[28]. The standard stipulates that an average of the 10 deepest pits and the maximum pit depth should be used for pit damage characterisation of the sample area.

2.5 X-ray diffraction

The XRD patterns for each sample were collected using a PANalytical X'pert multipurpose diffractometer (MPD), employing Cu Kα radiation with an active area of 10 x 10 mm^2. Scans were performed over a range 2θ = 20 to 80° using a step size of 0.033 per second, with a total scan time of approximately 50 minutes.

2.6 Scanning electron microscopy

SEM was carried out on samples using a Carl Zeiss EVO MA15 SEM to assess coverage and topography of corrosion product. All images were collected at an accelerating voltage of 20 kV and at a working distance of around 8 mm.

2.7 Raman spectroscopy

Raman spectra were collected by employing 488 nm radiation from an Ar ion laser (1% and 5%). The exposure time for each sample was recorded at between 5 and 30 minutes, with a total scan time of approximately 10 to 50 minutes. Raman spectroscopy was used to identify the nature of corrosion products locally on the surface and to detect the presence of potentially amorphous products not recorded by XRD.

3. Results and Discussion

3.1 General corrosion behaviour of X65 in CO_2/SO_2/H_2O system with varying concentrations of SO_2 and H_2O

Figure 2 shows the general corrosion rates (determined from mass loss measurements) of X65 samples exposed to the water-saturated and under-saturated supercritical CO_2 phase at

35°C and 80 bar, containing 0, 50 and 100 ppm of SO_2 for an immersion time of 48 hours. The corrosion rates are represented on both a logarithmic scale as well as a continuous scale to enable better interpretation of the data.

Figure 2 indicates that the general corrosion rate of X65 is low (<0.01 mm/year) in the presence of all three different concentrations of SO_2 when the water content is below 700 ppm. No corrosion was recorded in tests performed in dry, impure CO_2 i.e. with a water content of 0 ppm, as expected.

Referring to Figure 2, as the water concentration is increased, the general corrosion rate in each environment also rises. In all three conditions, an increase in water content from 300 to 1770 ppm resulted in an increase in general corrosion rate of ~0.003 to 0.07 mm/year. However, the increase in water content from 1770 ppm to water-saturated conditions caused more substantial rates of increase in corrosion rate. In tests containing 0, 50 and 100 ppm SO_2, general corrosion rates in the water-saturated environment reached 0.10, 0.37 and 0.72 mm/year, respectively. The effect of the presence of SO_2 becomes distinctly more noticeable as the water content in the system rises.

Referring to literature, the tests which are most comparable with the data produced here are those performed by Dugstad et al.[21] who evaluated the corrosion behaviour of carbon steel exposed to supercritical CO_2 at 20°C and 100 bar. In the presence of 200 ppm SO_2, 100 ppm O_2 and 488 ppm water, a general corrosion rate below 0.01 mm/year was recorded over 7 days of testing. This observation aligns well with the results in Figure 2, but it must be noted that there are differences in operating conditions and impurity concentrations between the two experiments.

In an additional publication, Dugstad et al.[1] conducted tests on X65 steel at 20°C and 100 bar in supercritical CO_2 for 14 days in a rotating system at 3 rpm. No attack was observed in the absence of SO_2 and O_2 at water contents of 488 and 1220 ppm water. However, the introduction of 100 ppm SO_2 at a water content of 488 ppm resulted in corrosion rates of <0.005 mm/year. Increasing SO_2 content further to 344 ppm and maintaining water content at 488 ppm resulted in the same general corrosion rate. Finally, a SO_2 content of 344 ppm and a higher water concentration of 1220 ppm increased the general corrosion rate to 0.02 mm/year. All these values align well with the observations recorded in Figure 2, despite the slight differences in operating temperature, pressure and impurity content.

Similarly, Choi and Nesic[20] performed tests with X65 steel exposed to supercritical CO_2 at 50°C and 80 bar for 24 hours in the presence of only 650 ppm water. They reported a corrosion rate below 0.01 mm/year, which aligns with the reported values here of ~0.004 mm/year at 700 ppm water under identical temperature and pressure.

3.2 Analysis of corrosion product morphology and composition

Figure 3 presents the scanning electron microscopy (SEM) images of the corroded X65 steel samples exposed to a selected number of conditions tested within the matrix in Table 5. Images of the steel surface exposed to 700 ppm water (Figures 3(a), (d) and (g)) showed minimal signs of corrosion on the steel surface. As water content is increased, the quantity of visible corrosion product on the steel surface became noticeably larger.

In the system exposed to supercritical CO_2 without the presence of SO_2 or O_2 (Fgures 3(a) – (c)), an increase in water content resulted in the formation of cubic crystals on the steel surface. These crystals were confirmed as $FeCO_3$ by XRD analysis. The resulting patterns can be observed in Figure 4 and the formation of such crystals is consistent with the observations of numerous authors[13, 16, 18, 25] in very similar environments.

In terms of the reaction mechanisms associated with the formation of $FeCO_3$, three series of reactions are capable within steel pipelines which transport supercritical CO_2 when water condenses onto the steel surface. These reactions are:

a) The saturation of the condensed water with CO_2, its association to produce carbonic acid and its subsequent partial homogenous dissociation in two steps to form bicarbonate and carbonate ions[11]:

$$\mathrm{CO_{2(g)}} \leftrightarrow \mathrm{CO_{2(aq)}} \tag{2}$$

$$\mathrm{CO_{2(g)} + H_2O_{(l)}} \leftrightarrow \mathrm{H_2CO_{3(aq)}} \tag{3}$$

$$\mathrm{H_2CO_3} \leftrightarrow \mathrm{H^+ + HCO_3^-} \tag{4}$$

$$\mathrm{HCO_3^-} \leftrightarrow \mathrm{H^+ + CO_3^{2-}} \tag{5}$$

b) In the next stage of reactions, the cathodic reaction can occur either by direct reduction of hydrogen ions, or the reduction of carbonic acid or carbonate ions[11]:

$$\mathrm{2H^+ + 2e^- \leftrightarrow H_2} \tag{6}$$

$$\mathrm{2H_2CO_3 + 2e^- \rightarrow H_2 + 2HCO_3^-} \tag{7}$$

$$\mathrm{2HCO_3^- + 2e^- \rightarrow H_2 + 2CO_3^{2-}} \tag{8}$$

c) The final stage is the anodic dissolution of iron:

$$Fe \rightarrow Fe^{2+} + 2e^{-} \quad (9)$$

Which can be followed by the precipitation of $FeCO_3$ via a one stage reaction with carbonates, or via a two stage reaction with bicarbonates[11]:

$$Fe^{2+} + CO_3^{2-} \rightarrow FeCO_3 \quad (10)$$

$$Fe^{2+} + 2HCO_3^{-} \rightarrow Fe(HCO_3)_2 \quad (11)$$

$$Fe(HCO_3)_2 \rightarrow FeCO_3 + CO_2 + H_2O \quad (12)$$

The introduction of both 50 and 100 ppm SO_2 with 20 ppm O_2 into the system resulted in the corrosion product morphology on the steel surface changing dramatically. Figures 3 (e), (f), (h) and (i) indicate that the presence of SO_2 initiated the formation of a thin, sulphur-containing compound (confirmed via EDX measurements) across the steel surface (whilst at higher water contents, the presence of columnar crystals was also observed (Figures 3(f) and(i)) which also possessed a high sulphur content. Both these types of surface morphology have been observed by Choi et al.,[13] at operating conditions of 80 bar and 50°C in water-saturated supercritical CO_2 in the presence of 0.8 bar SO_2 and 0.8 bar SO_2 with 3.3 bar O_2. In addition, to these observations, Figure 3(i) shows that these particular tests produced globular crystals on the steel surface which possessed no trace of elemental sulphur.

The XRD patterns for the sample exposed to the water-saturated environments containing 50 and 100 ppm SO_2 provided in Figure 4 confirmed that the sulphur-containing crystals are hydrated iron sulphite ($FeSO_3 \cdot 3H_2O$). The presence of $FeCO_3$ was also detected on the steel surface through XRD measurements. The use of localised Raman spectroscopy at specific locations on the steel surface (Figure 5) confirmed that the globular crystals were $FeCO_3$ and that the columnar crystals were $FeSO_3 \cdot 3H_2O$. The strongest Raman peak observed at 1085 cm^{-1} over the globular crystals in Figure 5 is representative of $FeCO_3$. Other peaks corresponding to the CO_3^{2-} are located at 735 cm^{-1} and 1500 cm^{-1}.

The strongest Raman peak observed from the scan over the globular crystals exists at 954 cm^{-1} for crystal $FeSO_3$ and the vibrational wavenumbers between ~3200 and 3400 cm^{-1} are related to the degree of hydration. As mentioned, the detection of $FeSO_3$ crystals is consistent with Choi et al.[13]. In their specific tests, no presence of $FeCO_3$ was recorded (potentially due to the high SO_2 content of 1% which may have preferred to form $FeSO_3$ in comparison to the formation of $FeCO_3$). The tests performed here have shown that the lower

320 SO_2 content (50 and 100 ppm) used in this study resulted in the co-presence of $FeCO_3$ and
321 $FeSO_3.3H_2O$ on the steel surface.

322 The formation of $FeSO_3$ can be described by the following reactions:
323
324 a) Firstly, SO_2 is believed to dissolve into the condensed water film on the surface and
325 subsequently becomes ionised:

$$H_2O + SO_2 \rightarrow H^+ + HSO_3^{2-} \quad (13)$$

$$HSO_3^{2-} \rightarrow H^+ + SO_3^{2-} \quad (14)$$

326 b) The cathodic reaction then occurs through the direct reduction of hydrogen ions:

$$2\mathrm{H}^+ + 2\mathrm{e}^- \leftrightarrow \mathrm{H}_2 \quad (15)$$

327 c) $FeSO_3$ then forms via a precipitation process:

$$Fe^{2+} + SO_3^{2-} \rightarrow FeSO_3 \quad (16)$$

328 Both Choi et al.[13] and Xiang et al.[23] have observed $FeSO_3$ in experiments involving SO_2,
329 however, in tests containing O_2 (1000 ppm in a 100 bar CO_2 system in the case of Xiang et
330 al.[23] and 3.3 bar partial pressure in a 80 bar CO_2 system in the case of Choi et al.[13], iron
331 sulphate ($FeSO_4$) was also detected. It was suggested that the addition of O_2 not only results
332 in an additional cathodic reaction, but it also enables the oxidation of sulphite ions to
333 sulphate ions, allowing $FeSO_4$ to form via a precipitation reaction[13]. It is apparent that the
334 low concentration of 20 ppm O_2 administered in these tests was not sufficient enough to
335 form appreciable amounts (if any) of $FeSO_4$ as it could not be detected through XRD or
336 Raman spectroscopy.

337
338 ***3.3 Localised corrosion measurements***

339 Figure 6 provides examples of the profilometry measurements from the sample surfaces
340 exposed to the under-saturated and water-saturated environment at 35°C and 80 bar with
341 concentrations of 0, 50 and 100 ppm SO_2 present in the system. The images indicate that
342 the presence of SO_2 has a significant effect on the extent of localised attack and is capable
343 of initiating more severe degradation at lower water contents than that in the absence of SO_2
344 and O_2. Profilometry measurements such as those displayed in Figure 6 were performed
345 numerous times on the surface of each steel sample. In some instances (e.g. under-
346 saturated conditions) all regions of localised attack could be easily focused on by the

profilometer. In other experiments where the surface degradation was more extensive, multiple measurements were performed on randomly chosen areas of the corroded steel surface in order to help accurately quantify the extent of localised attack. From all the profilometry scans collected on each sample surface, a multi-region analysis technique was employed to determine the top 10 deepest surface pits in accordance with ASTM Standard G46-94[28]. The pit depths were then converted to pitting rates based on exposure time to provide a quantitative assessment of the extent of localised attack.

The pitting rates produced from the profilometry assessment are provided in Figure 7 on both a logarithmic scale (Figure 7(a)) and a continuous scale (Figure 7(b)). The results show that localised corrosion rates can become appreciably high (in excess of 1 mm/year) if enough water is present in the system, even in the absence of SO_2 and O_2. In all three environments evaluated, corrosion rates exceeded 0.1 mm/year at a water content of 700 ppm. Only tests performed at 0 and 300 ppm water content produced no measureable localised attack on the steel surface. Interestingly, the most significant increase in pitting rate was observed between 1200 and 1770 ppm, whilst the largest increase in general corrosion was from 1770 ppm to water-saturated conditions.

These observations suggest that the minimum water content to produce acceptable levels of general corrosion differs dramatically from that required to prevent significant localised attack.

3.4 Establishing a critical water content – general vs localised corrosion assessment

Figure 8 shows 3D surface plots to indicate the variation in general and localised corrosion of X65 as a function of SO_2 and water content at 35°C and 80 bar. Both plots clearly indicate that increasing concentrations of SO_2 and water results in an increase in degradation rate. It is also clear that adhering to a maximum critical water content over a range of SO_2 concentrations is more effective than limiting SO_2 content, as degradation rates can still be excessive in high water contents without the presence of any SO_2.

Both Figures 8(a) and 8(b) show that a critical water content does exist, below which no substantial level of general or localised corrosion occurs. However, it is obvious that the critical water content required to minimise localised attack is considerably lower than that to reduce general corrosion to acceptable levels demonstrating that evaluating pitting rates is crucial in determining the safe conditions for CO_2 transport.

Figure 9 considers the water content required to reduce general and localised corrosion to below 0.1 mm/year based on the trends observed on the surface plots. These values were obtained through linear interpolation between the two measurements and as such, should not be regarded as exact values. Nonetheless, they illustrate an important point. The critical water content required to evaluate pitting rates is in crucial in determining the safe conditions for CO_2 transport.

In all three conditions, the water content required to prevent significant localised attack was established at approximately 500 ppm. However, the critical water content to reduce general corrosion to 0.1 mm/year varied and reduced significantly from 3400 to 1850 ppm as SO_2 content was increased from 0 to 100 ppm.

It is believed that for metals in corrosive environments, a critical relative humidity exists[29, 30], above which metal corrosion rate would experience a dramatic increase. The value of the critical humidity at atmospheric pressure is believed to be around 60-70%[24] and is potentially the reason behind some experts recommending an upper humidity level of 60% for supercritical CO_2 as a worst case scenario[7].

The only currently published study to consider this critical water content in high pressure CO_2 is that performed by Xiang et al.[24] who identified the critical relative humidity for the corrosion of X70 carbon steel in supercritical CO_2 at 100 bar and 50°C over 5 day experiments. These experiments were performed in the presence of 2% (2 bar) SO_2 and 1000 ppm O_2 at a rotation speed of 120 rpm. From mass loss measurements, Xiang et al.[24] determined the general corrosion rate of X70 as a function of humidity and established a very similar trend to that observed in Figure 2(b) consisting of low corrosion rates at low humidity, followed by a rapid rise once a critical water content was reached. Xiang et al.[24] reported that the critical humidity was approximately 50-60% based on the general corrosion rates determined from mass loss measurements. According to Figure 2(b), the general corrosion rate measurements tend to agree with the observation of Xiang et al.,[24], whereas the localised corrosion rates present a difference perspective by suggesting a considerably lower critical humidity.

It is important to state that it is unclear whether the pitting rates determined over 48 hours continue at this rate indefinitely. i.e. remain constant for the duration of the experiment. However, the measurements of high localised corrosion rates are in agreement with the observation by Farelas et al.[22] who recorded initial localised corrosion rates in excess of 2.4 mm/year for X65 samples exposed to liquid CO_2 at 25°C and 80 bar for 24 hours in under-saturated conditions in the presence of 650 ppm water and 0.05-0.1% SO_2. The growth of surface pits in such conditions will be the subject of further studies.

3.5 Fluids velocity

The velocity of the process fluid in dense phase CO_2 systems has been shown to influence the corrosion behaviour of materials[31] and it is perhaps worth commenting on the difference between the static tests performed in this study and how this compares to a dynamic system.

In fact, specific research[31] has suggested that the presence of flow within the system reduces the amount of water condensed onto the steel surface through entrainment back into the bulk solution and subsequently minimises the level of corrosion. Consequently, the results presented in this study in static conditions could be regarded as providing a worst case scenario in terms of corrosion rates, although this required further study.

In terms of supporting the theory of the surface velocities potentially producing lower corrosion rates, the work of Farelas et al.,[31] demonstrated that the presence of flow (1000 rpm sample rotation speed) reduced corrosion rates of X65 steel by around an order of magnitude in specific dense phase CO_2 environments. Farelas et al.,[31] performed tests at 80 bar in both liquid (25°C) and supercritical (50°C) conditions with the addition of 650 ppm water and 0.08 bar (0.1 %) SO_2. General corrosion rates reduced as the transition was made from static to dynamic from 0.03 to 0.02 mm/year in supercritical conditions and from 0.1 to 0.01 mm/year in liquid CO_2.

3.6 Consumption of impurities

One final point to note is that one of the issues associated with experiments in closed systems with low impurity concentrations is that significant levels of depletion can occur in the system over the course of the experiment. Based on the assumption that 1 mole impurity (water or SO_2) reacts with 1 mole Fe, the depletion of impurity can be estimated from the sample corrosion rate. The calculation requires the assumption that all corrosion is attributed to SO_2 and not carbonic acid. With this in mind, the rate of impurity depletion for SO_2 and water is provided in Figure 10.

Figure 10 indicates that significant consumption of the SO_2 occurred in tests where the water content was high. This poses the possibility that the corrosion rates recorded from mass loss measurements and surface profilometry did not provide a ‘worst case scenario’ corrosion rate in terms of CO_2 pipeline transportation.

As water content is reduced, the reduction in corrosion rate of the X65 steel results in the calculated loss of SO_2 in the system declining significantly. Below a water content of 700

448 ppm, the consumption of SO_2 was below 3%. Therefore, confidence exists in the accuracy of
449 the critical water contents stated in this study to minimise localised corrosion as at low water
450 contents, the level of depletion of impurities is reduced significantly.

451 In a publication by Dugstad et al.[1] it was stated that the actual consumption of impurities
452 had been studied in autoclave experiments by IFE. They suggested that typically, the
453 consumption of less than 5% impurities was sufficient to influence the corrosion rate.
454 Consequently, understanding the consumption of impurities in closed systems is imperative
455 in order to define acceptable CO_2 specifications with the utmost confidence.

456 **4. Conclusions**

457 The extent of general and localised corrosion of X65 steel in pure and impure supercritical
458 CO_2 is reviewed. Tests were performed in dense phase CO_2 containing small concentrations
459 of water (0 ppm to water-saturated CO_2), SO_2 (0-100 ppm) and O_2 (0-20 ppm) at 35°C and
460 80 bar for 48 hours in an effort to determine the effect of impurities on the critical water
461 content required to avoid significant levels of general and localised corrosion. The main
462 conclusions from this study are:

463 1. Corrosion of carbon steel can take place in conditions where the water content is well
464 below the solubility limit of water in supercritical CO_2 (300 ppm within this study) in
465 the presence of 0, 50 and 100 ppm SO_2. From this perspective, the molar
466 concentration limit of 500-650 ppm (DYNAMIS[7]/Kinder Morgan[5]) would not be
467 sufficient to completely prevent corrosion in a system at 35°C, although general
468 corrosion rates would be very small in such environments (i.e. below 0.04 mm/year).
469 2. Increasing water content resulted in an increase in corrosion rate in all test
470 environments. In the absence of SO_2 and O_2, the critical water content at which a
471 general corrosion rate of 0.1 mm/year was reached was determined to be 3400 ppm,
472 which was very close to the solubility limit of water in CO_2 under the given conditions.
473 3. The introduction of 50 ppm SO_2 and 20 ppm O_2 resulted in a significant reduction in
474 the critical water content required to stay below a general corrosion rate of 0.1
475 mm/year, reducing it to ~2120 ppm. Further increase in SO_2 content to 100 ppm,
476 reduce the critical water content to ~1850 ppm.
477 4. Profilometry measurements indicated significant levels of localised attack on the steel
478 surface, predominantly in the form of pitting. The attack became more prominent with
479 increasing SO_2 and water content.
480 5. The critical water content required to minimise significant level of localised attack was
481 substantially lower than that required to prevent general corrosion (0.1 mm/year) and

was determined to be approximately 500 ppm, irrespective of SO_2 content (0, 50 or 100 ppm).

6. The results indicated that minimising water content is a better strategy compared to reducing SO_2 content as a method to reduce both general and localised corrosion as substantial corrosion was still observed at high water contents in the absence of SO_2 and O_2.
7. Calculations of impurity consumption indicated that water and SO_2 consumption was excessive in high humidity environments. However, consumption was below 5% in conditions near the critical water content to minimise localised corrosion. Therefore, this promoted confidence in the results at low water content, but suggested the values obtained at high water content may not reflect the 'worst case scenario' corrosion rate.

5. References

1. A. Dugstad, M. Halseid, and B. Morland, *Effect of SO_2 and NO_2 on corrosion and solid formation in dense phase CO_2 pipelines.* Energy Procedia, 2013. **37**: p. 2877-2887.
2. F.W. Schremp and R.G. Roberson, "*Effect of Supercritical Carbon Dioxide (CO_2) on Construction Materials*".
3. A. Oosterkamp and J. Ramsen, *State-of-the-art overview of CO_2 pipeline transport with relevance to offshore pipelines.* Polytech Report No: POL-O-2007-138-A, 2008.
4. J. Gale and J. Davison, *Transmission of CO_2—safety and economic considerations.* Energy, 2004. **29**(9–10): p. 1319-1328.
5. Kinder Morgan. Available from: http://www.kindermorgan.com/business/co2/transport.cfm.
6. D.E. McCollough and R.L. Stiles, "*Operation of the Central Basin CO_2 Pipeline System*", Society of Petroleum Engineers.
7. E.D. Visser, C. Hendriks, M. Barrio, M.J. Mølnvik, G.D. Koeijer, S. Liljemark, and Y.L. Gallo, *Dynamis CO_2 quality recommendations.* International Journal of Greenhouse Gas Control, 2008. **2**(4): p. 478-484.
8. T. Maldal and I.M. Tappel, *CO_2 underground storage for Snøhvit gas field development.* Energy, 2004. **29**(9): p. 1403-1411.
9. M.E. Boot-Handford, J.C. Abanades, E.J. Anthony, M.J. Blunt, S. Brandani, N. Mac Dowell, J.R. Fernandez, M.-C. Ferrari, R. Gross, J.P. Hallett, R.S. Haszeldine, P. Heptonstall, A. Lyngfelt, Z. Makuch, E. Mangano, R.T.J. Porter, M. Pourkashanian, G.T. Rochelle, N. Shah, J.G. Yao, and P.S. Fennell, *Carbon capture and storage update.* Energy & Environmental Science, 2014. **7**(1): p. 130-189.
10. J.-Y. Lee, T.C. Keener, and Y.J. Yang, *Potential flue gas impurities in carbon dioxide streams separated from coal-fired power plants.* Journal of the Air & Waste Management Association, 2009. **59**(6): p. 725-732.

11. I.S. Cole, P. Corrigan, S. Sim, and N. Birbilis, *Corrosion of pipelines used for CO_2 transport in CCS: Is it a real problem?* International Journal of Greenhouse Gas Control, 2011. **5**(4): p. 749-756.

12. A. Aspelund and K. Jordal, *Gas conditioning—The interface between CO< sub> 2</sub> capture and transport.* International Journal of Greenhouse Gas Control, 2007. **1**(3): p. 343-354.

13. Y.-S. Choi, S. Nešić, and D. Young, *Effect of impurities on the corrosion behavior of CO_2 transmission pipeline steel in supercritical CO_2−water environments.* Environmental Science & Technology, 2010. **44**(23): p. 9233-9238.

14. Y. Xiang, Z. Wang, Z. Li, and W.D. Ni, *Effect of Exposure Time on the Corrosion Rates of X70 Steel in Supercritical CO_2/SO_2/O_2/H_2O Environments.* Corrosion, 2012. **69**(3): p. 251-258.

15. A. Dugstad, S. Clausen, and B. Morland, "*Transport of dense phase CO_2 in C-steel pipelines - when is corrosion an issue?*", in *CORROSION 2011*. 2011: Houston, TX:NACE.

16. Y. Hua, R. Barker, and A. Neville, *Effect of temperautre on the critical water content for general and localised corrosion of X65 carbon steel in the transport of supercritical CO_2.* The International Journal of Greenhouse Gas Control, 2014. **31**: p. 48-60.

17. Y. Hua, R. Barker, and A. Neville, *Comparison of corrosion behaviour for X-65 carbon steel in supercritical CO2-saturated water and water-saturated/unsaturated supercritical CO2* The Journal of Supercritical Fluids, 2015. **97**: p. 224-237.

18. Y. Hua, R. Barker, C. T, M. Ward, and A. Neville, *Relating Iron Carbonate Morphology to Corrosion Characteristics for Water-Saturated Supercritical CO2 Systems.* The Journal of Supercritical Fluids, 2014: p. Article In Press.

19. S. Sim, F. Bocher, I.S. Cole, X.B. Chen, and N. Birbilis, *Investigating the effect of water content in supercritical CO_2 as relevant to the corrosion of carbon capture and storage pipelines.* Corrosion, 2014. **70**(2): p. 185-195.

20. Y.-S. Choi and S. Nesic, "*Effect of water content on the corrosion behavior of carbon steel in supercritical CO_2 phase with impurities*", in *CORROSION 2011*. 2011: Houston, TX:NACE.

21. A. Dugstad, B. Morland, and S. Clausen, *Corrosion of transport pipelines for CO_2– Effect of water ingress.* Energy Procedia, 2011. **4**: p. 3063-3070.

22. F. Farelas, Y.-S. Choi, and S. Nešić, *Corrosion Behavior of API 5L X65 Carbon Steel under Supercritical and Liquid Carbon Dioxide Phases in the Presence of Water and Sulfur Dioxide.* Corrosion, 2012. **69**(3): p. 243-250.

23. Y. Xiang, Z. Wang, C. Xu, C.C. Zhou, Z. Li, and W.D. Ni, *Impact of SO_2 concentration on the corrosion rate of X70 steel and iron in water-saturated supercritical CO_2 mixed with SO_2.* The Journal of Supercritical Fluids, 2011. **58**(2): p. 286-294.

24. Y. Xiang, Z. Wang, X.X. Yang, Z. Li, and W.D. Ni, *The upper limit of moisture content for supercritical CO_2 pipeline transport.* The Journal of Supercritical Fluids, 2012. **67**: p. 14-21.

25. Y. Hua, R. Barker, and A. Neville, *Understanding the Influence of SO2 and O2 on the Corrosion of Carbon Steel in Water-Saturated Supercritical CO2.* Corrosion, 2014: p. Article In Press.

26. N. Spycher, K. Pruess, and J. Ennis-King, *CO_2-H_2O mixtures in the geological sequestration of CO_2. I. Assessment and calculation of mutual solubilities from 12 to*

570 *100°C and up to 600 bar.* Geochimica et Cosmochimica Acta, 2003. **67**(16): p. 3015-
571 3031.

572 27. ASTM. Standard G1-03, Standard practice for preparing, cleaning, and evaluating
573 corrosion test specimens. ASTM International: West Conshohocken, PA, 2003.

574 28. ASTM. Standard G46-94, Standard guide for examination and evaluation of pitting
575 corrosion. ASTM International: West Conshohocken, PA, 2003.

576 29. W.H.J. Vernon, *A laboratory study of the atmospheric corrosion of metals. Part II.—*
577 *Iron: the primary oxide film. Part III.—The secondary product or rust (influence of*
578 *sulphur dioxide, carbon dioxide, and suspended particles on the rusting of iron).*
579 Transactions of the Faraday Society, 1935. **31**: p. 1668-1700.

580 30. W.H.J. Vernon, *A laboratory study of the atmospheric corrosion of metals. Part I.—*
581 *The Corrosion of copper in certain synthetic atmospheres, with particular reference to*
582 *the influence of sulphur dioxide in air of various relative humidities.* Transactions of
583 the Faraday Society, 1931. **27**: p. 255-277.

584 31. F. Farelas, Y.-S. Choi, and S. Nesic, "*Effects of CO_2 phase change, SO_2 content and*
585 *flow on the corrosion of CO_2 transmission pipeline steel*", in *CORROSION 2012*.
586 2012: Salt Lake City, UT:NACE.

587 32. I.S. Cole, D.A. Paterson, P. Corrigan, S. Sim, and N. Birbilis, *State of the aqueous*
588 *phase in liquid and supercritical CO_2 as relevant to CCS pipelines.* International
589 Journal of Greenhouse Gas Control, 2012. **7**(0): p. 82-88.

590

591

592 **Table 1: CO_2 compositions transported in existing pipelines – adapted from McCollough and Stiles[6], de Visser et al.[7] Maldal and**
593 **Tappel[8] and Boot-Hanford et al.[9]**

	Canyon Reef Carriers[2, 3, 4, 5, 9]	Central Basin Pipeline[3, 5, 6, 9]	Sheep Mountain[4, 5, 9]	Bravo Dome Source[3, 4, 5, 9]	Cortez Pipeline[3, 4, 9]	Weyburn[7, 9]	Jackson Dome[3]	Sleipner[7, 9]	Snohvit[3, 8, 9]
Location	USA	USA	USA	USA	USA	USA and Canada	USA	Norway	Norway
Operator	Kinder Morgan	Kinder Morgan	BP	BP	Kinder Morgan	Dakota Gasification Company	Denbury Resources	Statoil	Statoil
Length (km)	352	278	772	350	803	328	295	153	160
Capacity (Mt/y)	4.4	20	9.2	7.3	19.3	5	n/a	0.7	1
Source	Anthropogenic - Gasification Plant	Natural	Natural	Natural	Natural	Anthropogenic - Gasification Plant	Natural	Separation from Natural Gas	Separation from Natural Gas
CO_2 (vol.%)	85-98	98.5	96.8-97.4	99.7	95	96	98.7-99.4	93-96	Not specified
CH_4 (vol.%)	2-15 (C_6H_{14})	0.2	1.7	-	1-5	0.7	0.3	0.5-2.0 total hydrocarbons	Not specified
N_2 (vol.%)	<0.5	1.3	0.6-0.9	0.3	4	<300 ppm	0.3	3-5 non-condensable	Not specified
H_2S	<260 ppm	<26 ppm	-	-	20 ppm	9000 ppm	-	150 ppm	Not specified
C_2+ (vol.%)	-	-	0.3-0.6	-	Trace	2.3	-	0.5-2.0 total hydrocarbons	Not specified
CO (vol.%)	-	-	-	-	-	0.1	-	-	Not specified
O_2	-	<14 ppm	-	-	-	<70 ppm	-	-	Not specified
NO_X	Not specified	-	-	-	-	Not specified	-	-	Not specified
SO_X	Not specified	-	-	-	-	Not specified	-	-	Not specified
H_2 (vol.%)	-	-	-	-	-	Trace	-	3-5 non-condensable	Not specified
Ar (vol.%)	-	-	-	-	-	-	-	3-5 non-condensable	Not specified
Water content	122 ppm	630 ppm	315 ppm	Not specified	630 ppm	20 ppm	418 ppm	Water-saturated (Corrosion Resistant Alloy pipeline)	50 ppm

Table 2: Typical performance values for removal of flue gas components by SO_x, NO_x and CO_2 control systems – adapted from Lee et al.[10] and Cole et al.[32]

	Contaminants				
	SO_2	**SO_3**	**NO_2**	**HCl**	**Hg^{2+}**
No contaminant control	0.6-4.4 wt.%	42-579 ppm	24-111 ppm	36-835 ppm	23-261 ppm
SO_2 control by a wet FGD scrubber	337-2403 ppm	21-302 ppm	18-87 ppm	2-44 ppm	2-27 ppm
NO_x control by LNB/SCR	0.6-4.4 wt.%	42-579 ppm	10-44 ppm	36-835 ppm	23-261 ppm
NO_x control by LNB/SCR plus SO_2 control by a wet FGD scrubber	337-2403 ppm	21-302 ppm	7-35 ppm	2-44 ppm	2-27 ppm
NO_x control by LNB/SCR plus SO_2 control by a wet FGD scrubber, and also assuming MEAS-based CO_2 control unit is used to trap CO_2	34-135 ppm	<(21-302) ppm	<(7-35) ppm	<(2-44) ppm	<(2-27) ppb

Note: FGD = flue gas desulphurisation, LNB = low NO_x burner, SCR = selective catalytic reduction

Table 3: Elemental composition of X65 steel (wt.%)

C	Si	Mn	P	S	Cr	Mo	Ni
0.12	0.18	1.27	0.008	0.002	0.11	0.17	0.07
Cu	**Sn**	**Al**	**B**	**Nb**	**Ti**	**V**	**Fe**
0.12	0.008	0.022	0.0005	0.054	0.001	0.057	Balance

600 **Table 4: DYNAMIS CO_2 quality recommendations and Alstom CO_2 quality tolerances**
601 **(the reasons behind each limitation is also provided)**

Component	DYNAMIC CO_2 quality recommendations (adapted from de Visser et al.[7])		Alstom CO_2 quality tolerances (adapted from Dugstad et al.[15])		
	Concentration Limit	**Reason for Limit**	**Low Limit**	**High Limit**	**Reason for Limit**
CO_2	>95.5 vol.%	Balanced with other compounds in CO_2	>90% vol.% (storage)	>95% vol.% (EOR)	Low – Storage requirement High – EOR requirement
N_2/Ar/ H_2	< 4 vol.%	As proposed in ENCAP	<4 vol.%		EOR requirement
O_2	Aquifer < 4 vol.%, EOR 100 – 1000 ppm	Technical: range for EOR due to lack of practical experiments on effect of O_2 underground	<10 ppm	<1000 ppm	Unclear
CH_4	Aquifer < 4 vol.%, EOR < 2 vol.%,	As proposed in ENCAP	<4%	<4%	EOR requirement
H_2O	500 ppm	Technical: below solubility limit of H_2O in CO_2. No significant cross effect of H_2O and H_2S, cross effect of H_2O and CH_4 is significant but within limits for water solubility.	<10 ppm	<600 ppm	Corrosion prevention requirement
H_2S	200 ppm	Health and Safety	<10 ppm	<15000 ppm	Low – Health and Safety High – EOR requirement
CO	2000 ppm	Health and Safety	<100 ppm	<40000 ppm	Low – Health and Safety High – EOR requirement
SO_x	100 ppm	Health and Safety	<100 ppm	<1500 ppm	Low – Health and Safety High – EOR requirement
NO_x	100 ppm	Health and Safety	<100 ppm	<1500 ppm	Low – Health and Safety High - Unclear

602

603 **Table 5: Test matrix for corrosion experiments**

Water-saturated CO_2					
Temperature (°C)	**Pressure (bar)**	**H_2O (ppm)**	**SO_2 (ppm)**	**O_2 (ppm)**	**Immersion time (hours)**
35	80	Above solubility limit of 3437ppm through addition of 34000ppm water	0, 50, 100	20 (0 ppm for 0 ppm SO_2)	48
Under-saturated CO_2					
Temperature (°C)	**Pressure (bar)**	**H_2O (ppm)**	**SO_2 (ppm)**	**O_2 (ppm)**	**Immersion time (hours)**
35	80	1770	0, 50, 100	20 (0 ppm for 0 ppm SO_2)	48
		1200			
		700			
		300			
		0			

604

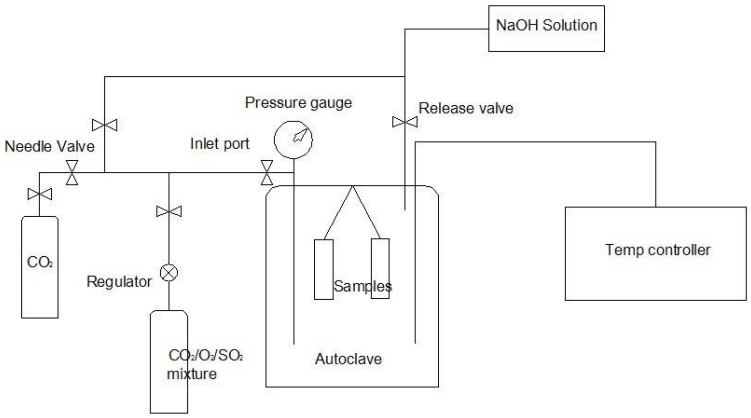

Figure 1: Schematic of autoclave setup

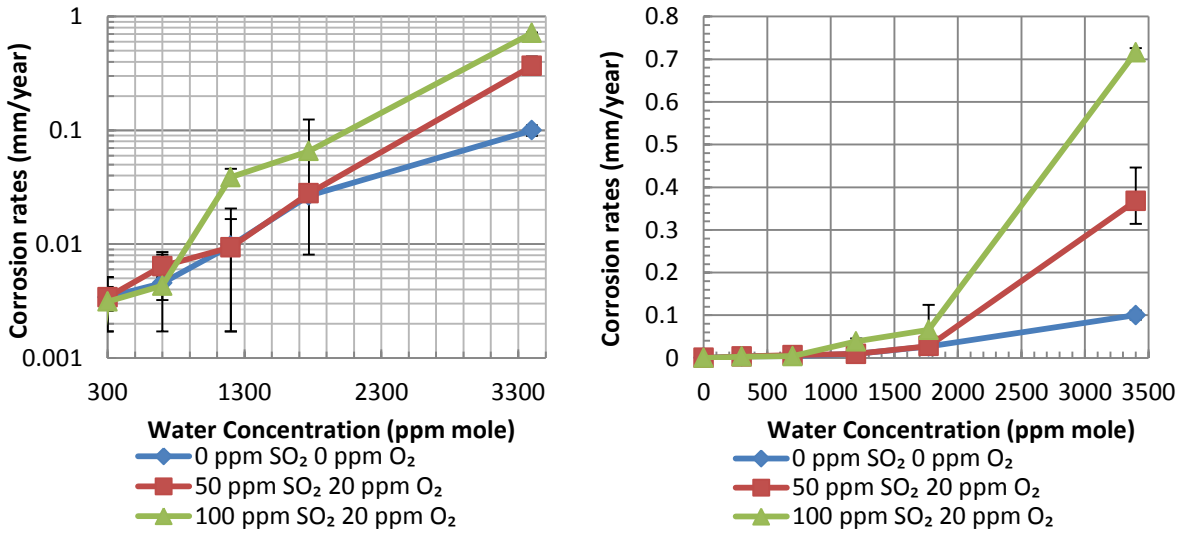

(a) **(b)**

Figure 2: Corrosion rates of X65 carbon steel in under-saturated and water-saturated CO_2 phase at 80 bar and 35°C over an exposure time of 48 hours. SO_2 in the gas phase is varied from 0 to 100 ppm. Data is presented on (a) a logarithmic scale and (b) a continuous scale

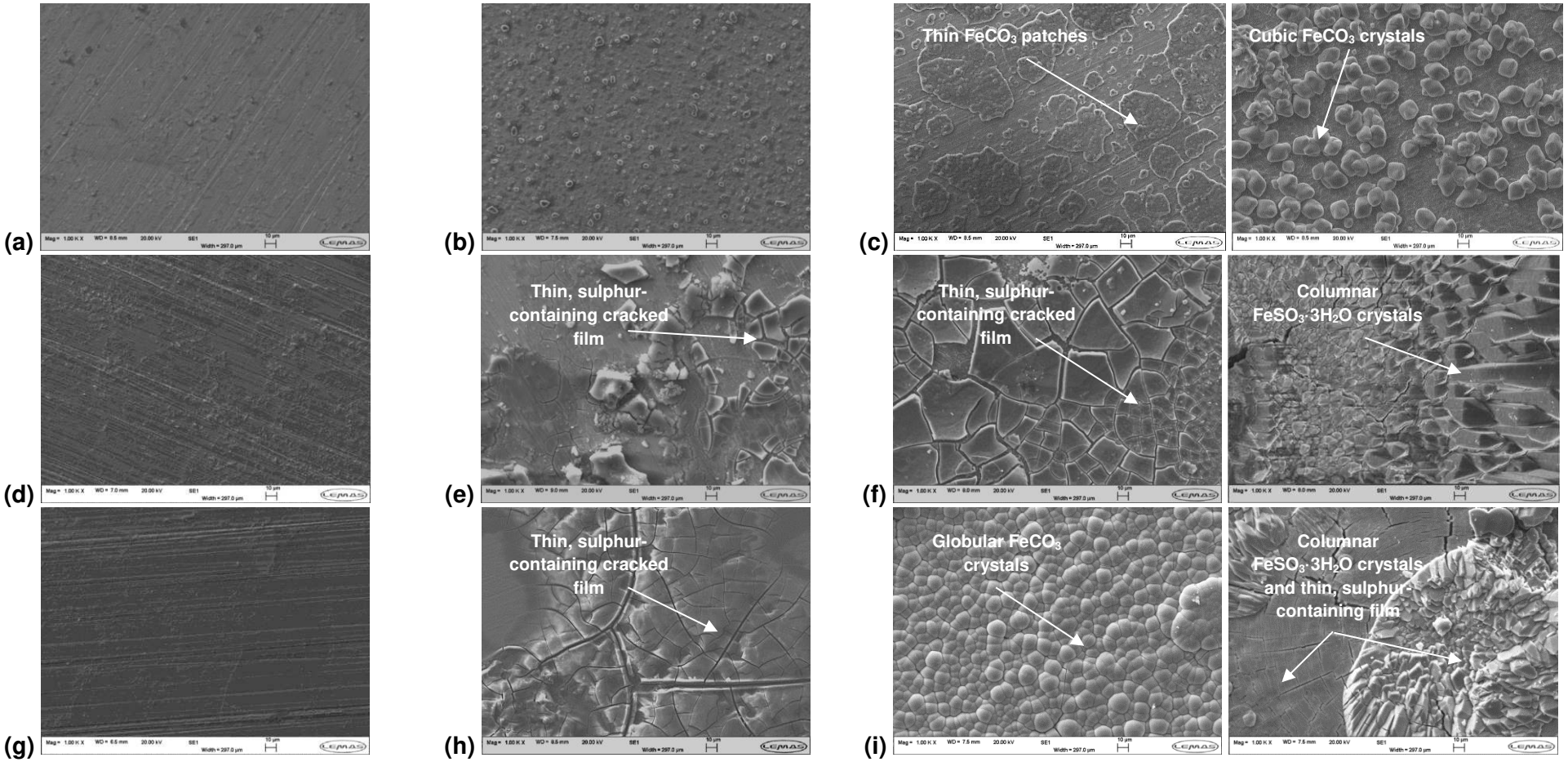

Figure 3: SEM images of the X65 corroded samples exposed to under-saturated and water-saturated CO_2 at 35°C and 80 bar for 48 hours in the presence of various concentrations of impurities; (a)-(c) 0 ppm SO_2 and 0 ppm O_2 in the presence of 700, 1770 and 3437 ppm (water-saturated) water, respectively; (d)-(f) 50 ppm SO_2 and 20 ppm O_2 in the presence of 700, 1770 and 3437 ppm (water-saturated) water, respectively; (g)-(i) 100 ppm SO_2 and 20 ppm O_2 in the presence of 700, 1770 and 3437 ppm (water-saturated) water, respectively

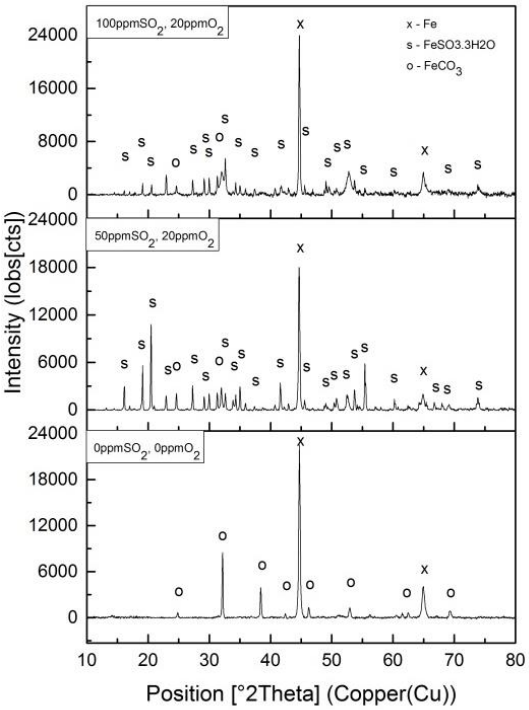

Figure 4: XRD spectra of samples exposed to water-saturated CO_2 phase at 35°C and 80 bar containing different concentration levels of SO_2 (0, 50 and 100 ppm) and O_2 (0 and 20 ppm) impurities

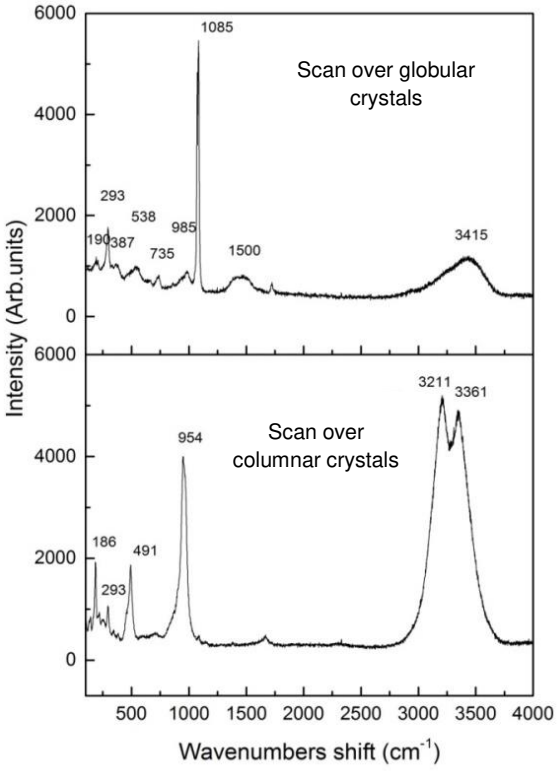

Figure 5: Raman spectra of samples exposed to water-saturated supercritical CO_2 phase at 35°C and 80 bar containing 100 ppm SO_2 and 20 ppm O_2. Areas scanned on the steel surface are representative of those depicted in Figure 3(i).

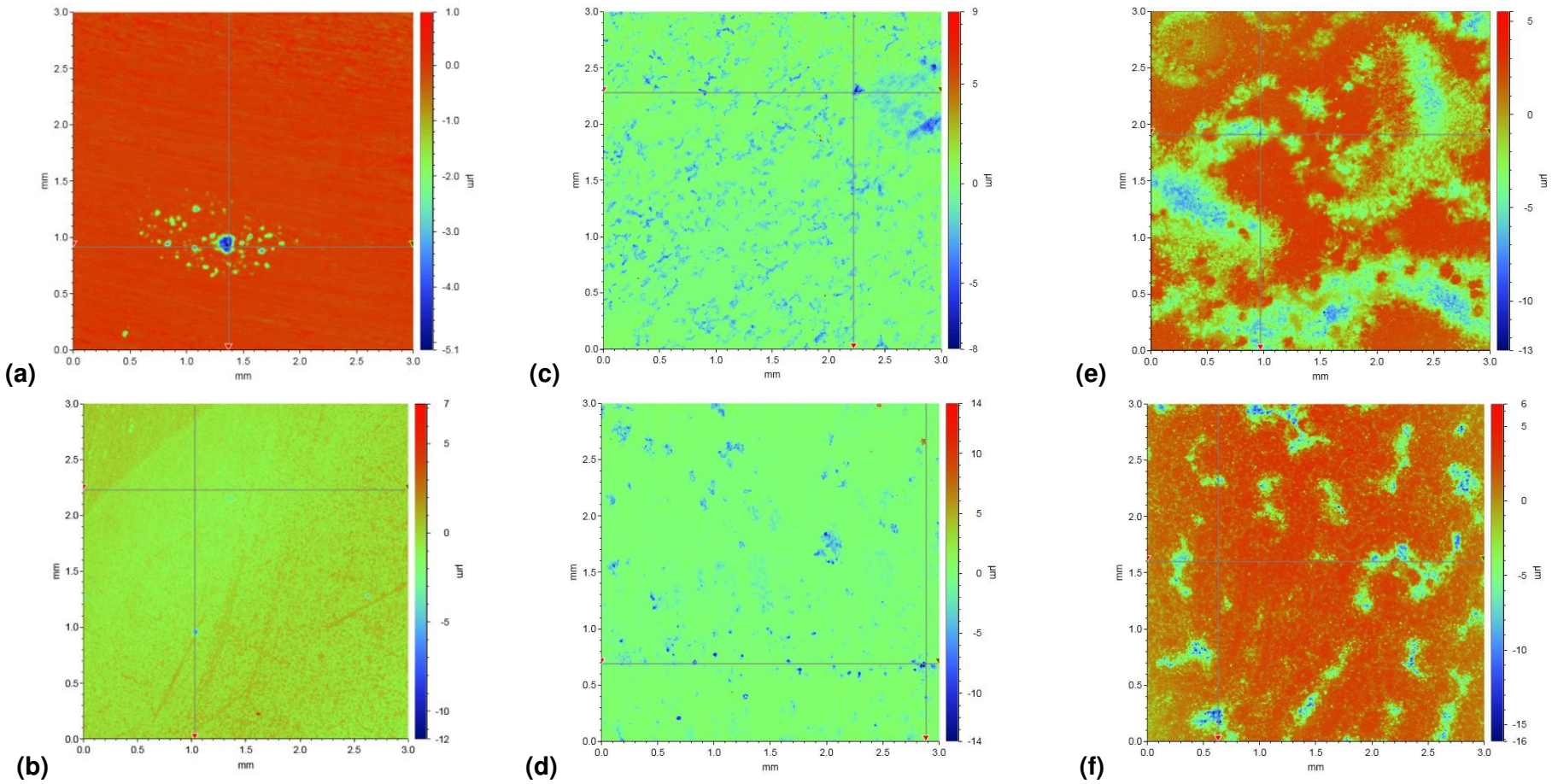

Figure 6: Example profilometry images of X65 steel surfaces after removal of corrosion products (a) 0 ppm SO_2, 0 ppm O_2, 1770 ppm water, (b) 0 ppm SO_2, 0 ppm O_2, water-saturated, (c) 50 ppm SO_2, 20 ppm O_2, 1770 ppm water, (d) 50 ppm SO_2, 20 ppm O_2, water-saturated, (e) 100 ppm SO_2, 20 ppm O_2, 1770 ppm water, (f) 100 ppm SO_2, 20 ppm O_2, water-saturated. All tests were performed at 35°C and 80 bar for 48 hours in supercritical CO_2.

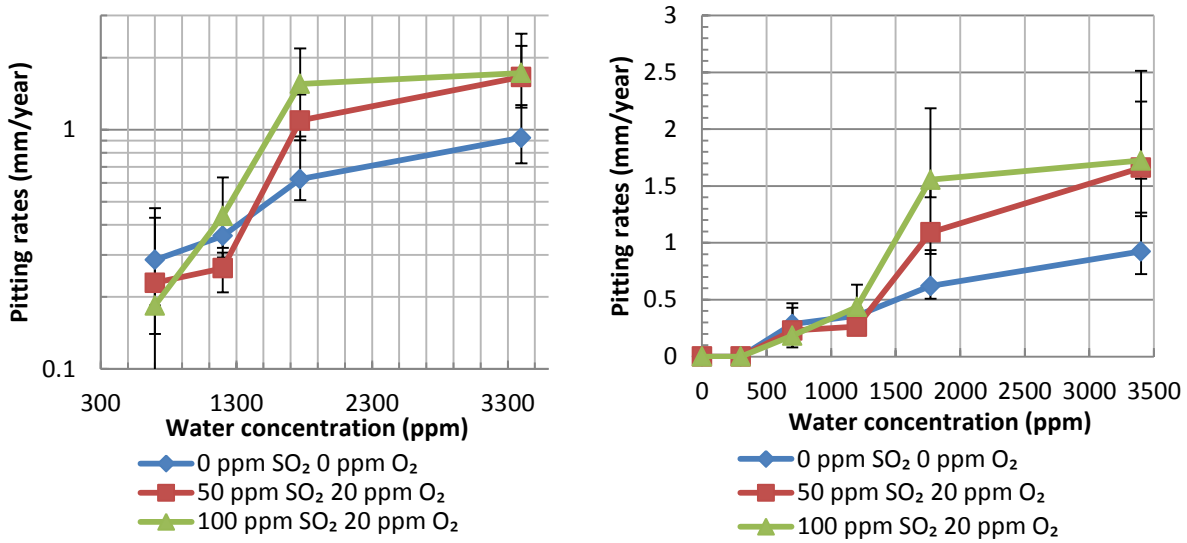

632

(a) (b)

633 **Figure 7: Pitting corrosion rates of X65 carbon steel in under-saturated and water-**
634 **saturated CO_2 phase at 80 bar and temperature of 35°C for an exposure time of 48**
635 **hours. SO_2 in the gas phase is varied from 0 to 100 ppm. Data is presented on (a) a**
636 **logarithmic scale and (b) a continuous scale**

637

638

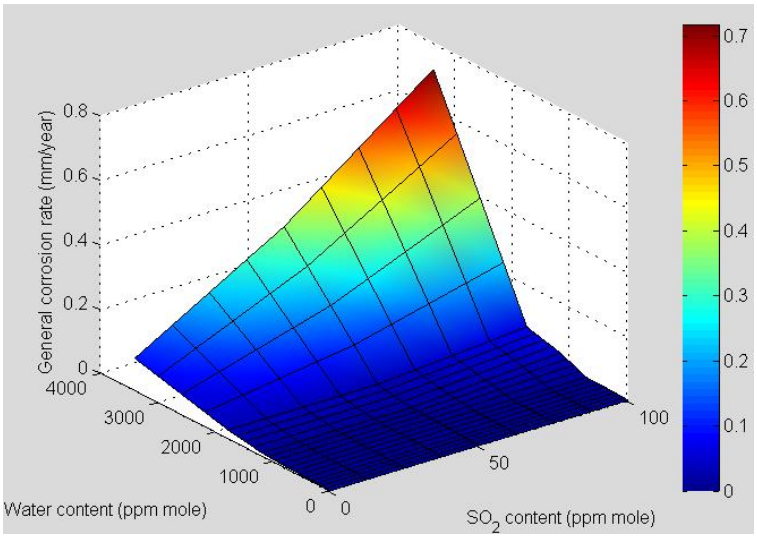

639

640 **(a)**

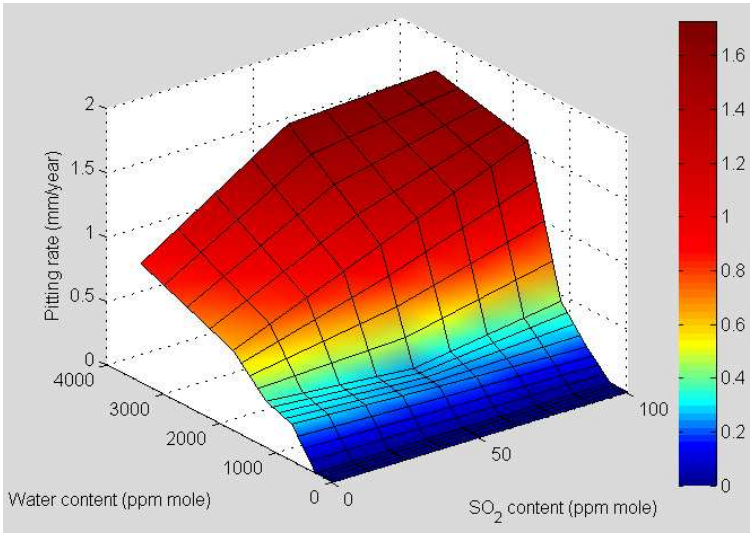

641

642 **(b)**

643 **Figure 8: Surface plots to indicate the variation of (a) general and (b) pitting/localised**
644 **corrosion rates as a function of SO_2 and water content. All tests were performed at**
645 **35°C and 80 bar.**

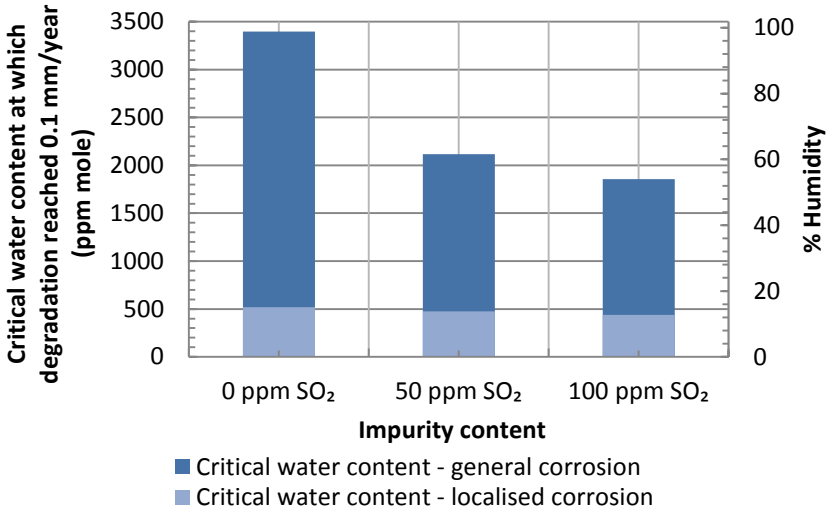

646

647 **Figure 9: Critical water content at which 0.1 mm/year corrosion rate is reached from**
648 **the perspective of general and localised corrosion for X65 steel. Conditions are 35°C**
649 **and 80 bar in supercritical CO_2 for 48 hours.**

650

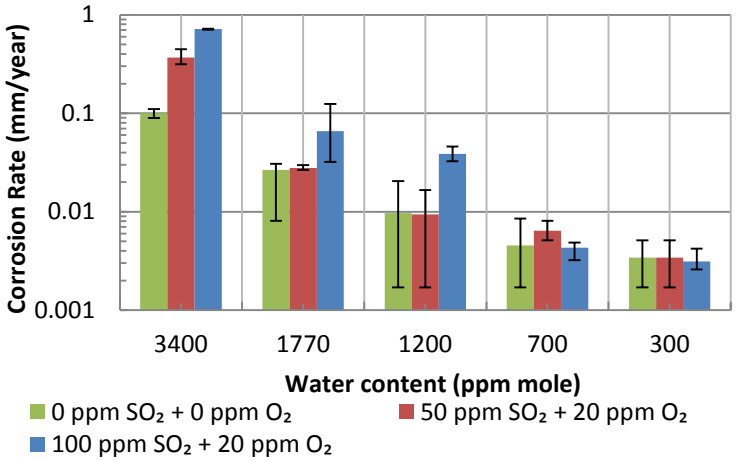

651

652 **(a)**

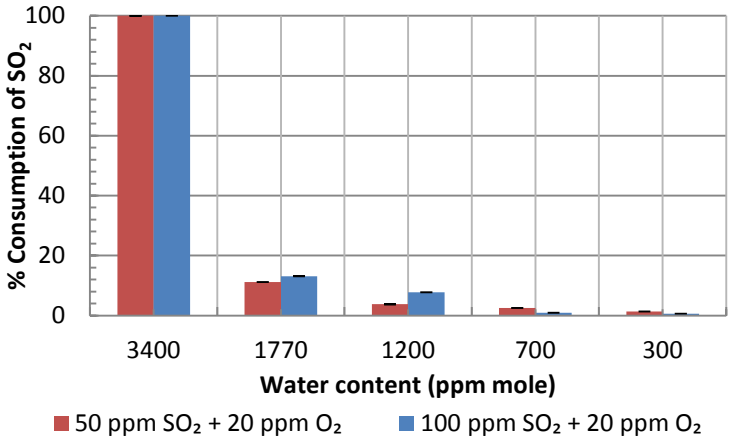

653

654 **(b)**

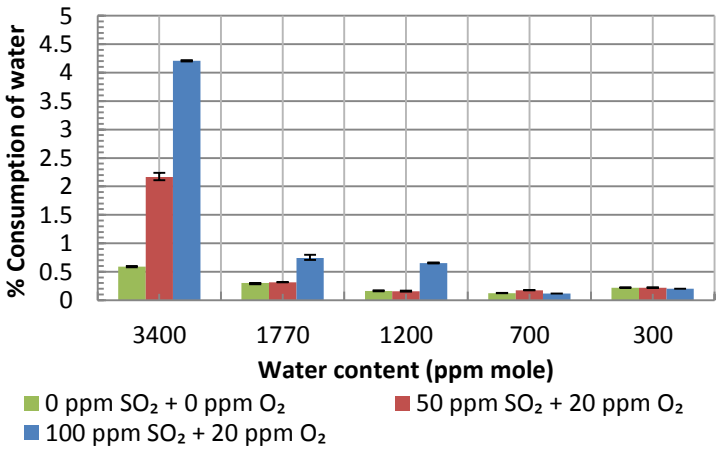

655

656 **(c)**

657 **Figure 10: (a) General corrosion rate and rate of consumption of (b) SO_2 and (c) water**

658 **under different conditions at 80 bar and 35°C**